JACS
JOURNAL OF THE AMERICAN CHEMICAL SOCIETY
pubs.acs.org/JACS
Article

Elemene Hydrogel Modulates the Tumor Immune Microenvironment for Enhanced Treatment of Postoperative Cancer Recurrence and Metastases

Jing Xian,[⊥] Fan Xiao,[⊥] Jianhua Zou, Wei Luo, Shiqi Han, Ziwei Liu, Yiquan Chen, Qianru Zhu, Meng Li, Chuao Yu, Qimanguli Saiding, Wei Tao,* Na Kong,* and Tian Xie*

Cite This: https://doi.org/10.1021/jacs.4c12531
Read Online

ABSTRACT: As a representative active ingredient of traditional Chinese medicine (TCM) and a clinically approved anticancer drug, elemene (ELE) exhibits exciting potential in the antitumor field; however, appropriate drug formulations still need to be explored for specific diseases such as postoperative cancer recurrence and metastasis. Herein, we report an ELE hydrogel with controlled drug release kinetics that can allow ELE to maintain effective concentrations at local lesion sites for extended periods to enhance the bioavailability of ELE. Concretely, dopamine-conjugated hyaluronic acid is synthesized and utilized to prepare ELE nanodrug-embedded hydrogels. In a model of postoperative breast cancer recurrence and metastasis, the ELE hydrogel demonstrates a 96% inhibition rate of recurrence; in contrast, the free ELE nanodrug shows only a 65.5% inhibition rate of recurrence. Importantly, the ELE hydrogel markedly stimulates a potent antitumor immune response in the microenvironment of cancer lesions, increasing antitumor immune cells such as $CD8^+$ T cells, $CD4^+$ T cells, and M1-type macrophages, as well as elevating antitumor cytokines including TNF-α, IFN-γ, and IL-6. Overall, this study not only advances the field of TCM but also highlights the transformative impact of controlled-release hydrogels in improving antitumor therapy.

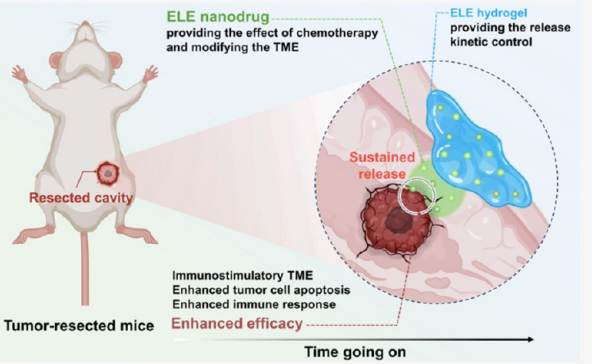

INTRODUCTION

Traditional Chinese medicine (TCM) is regarded as a precious repository that offers valuable therapeutic experiences and drug resources.[1,2] Artemisinin, discovered by Tu and her team, has saved millions of lives,[3,4] demonstrating the immense potential of TCM in treating major diseases. Specifically, elemene (ELE), another representative active ingredient derived from the Chinese herb *Curcuma wenyujin*, has demonstrated powerful antitumor effects in cancer treatment.[5] For example, our group utilized ELE as a model drug to investigate antitumor therapy.[6] Additionally, ELE can also be combined with other therapeutic strategies, such as ultrasound-mediated sonodynamic therapy,[7] nanosheet-mediated thermoelectric strategies,[8] cetuximab-mediated immunotherapy,[9] and arsenene/germanene/stanene-based chemotherapy,[10−12] as well as mRNA-based therapy, for antitumor therapy based on "molecular compatibility" theory,[13] demonstrating promising outcomes in antitumor therapy.[14] Recently, our group discovered that ELE can mediate the transformation of tumor-associated macrophages from M2-type to M1-type, playing a crucial role in immunotherapy strategies.[15]

The rapid advancement in materials science has propelled the modernization of TCM. For instance, advanced material platforms can be employed to effectively modify the drug release kinetics of active ingredients from TCM, thereby enhancing their final therapeutic efficacy.[16] The release kinetics of the drug influence the drug's duration and concentration at the lesion site.[17] By controlling the release kinetics, long-acting drug formulations can be designed to maintain effective concentrations over a sufficient duration, thereby improving the bioavailability of the drug, reducing dosing frequency, and enhancing treatment compliance.[18,19] Many studies have reported that controlled-release kinetics of drugs can be achieved by designing different drug formulations to enhance the therapeutic effects of drugs. Particularly, hydrogel and microneedles have been employed to control the release kinetics of drugs and further for the treatment of diseases including periodontal diseases, ocular disease, arthritis, and cancer postsurgical intervention.[20−24] For instance, commercial Ocusert offers a continuous local release of pilocarpine in the

Received: September 9, 2024
Revised: November 13, 2024
Accepted: November 14, 2024

Scheme 1. Schematic Illustration of (A) Release Kinetic Control of ELE Nanodrug and (B) Its Application in Preventing Cancer Postoperative Recurrence and Metastases[a]

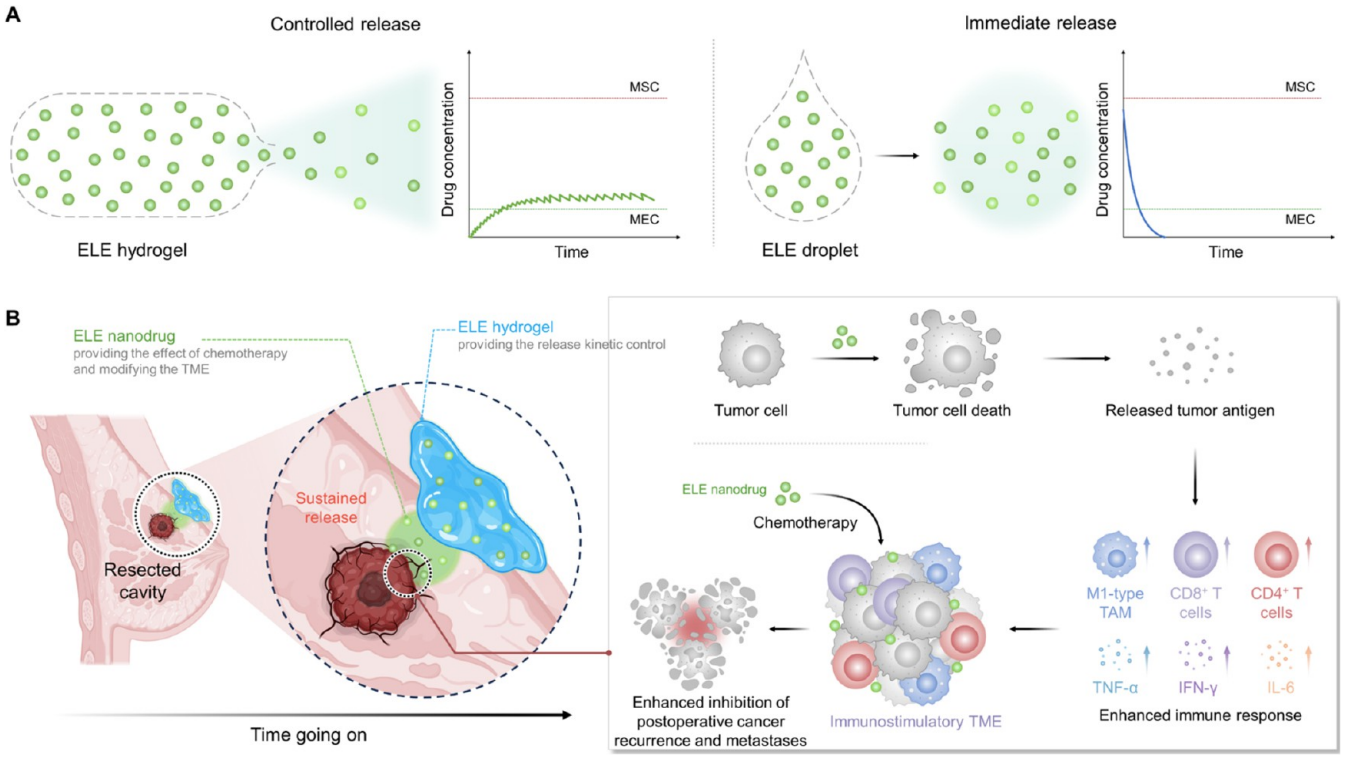

[a]MSC: maximum safe concentration, MEC: minimum effective concentration.

eye for 1 week, aiding in the treatment of glaucoma.[25,26] In recent studies, a thermosensitive hydrogel was used to coencapsulate BRAF inhibitor and aPD-1 intratumorally, prolonging the local drug release in the tumor, thereby greatly improving the local immune response and tumor inhibition.[27] Besides, an injectable hydrogel was reported to manipulate the release profile of nanodrug for postsurgical brain tumor treatment.[28] In another example, iron nanochelator-loaded hydrogel altered the release kinetics of deferoxamine, eventually mitigating high iron symptoms.[29] Collectively and, therefore, it is attractive to control the release kinetics of ELE to enhance its ultimate therapeutic effect.

Herein, an ELE hydrogel with controlled-release profiles (Scheme 1) is developed to maintain effective concentrations of ELE over time, thus exerting enhanced therapeutic effects. Specifically, a dopamine-conjugated hyaluronic acid system was employed to prepare a hydrogel with controlled-release kinetics, and embedded ELE nanodrug within it. We demonstrated that the ELE hydrogel can significantly inhibit postoperative recurrence and lung metastasis in breast cancer. Notably, compared with the ELE nanodrug drops, the ELE hydrogel markedly altered the immune cell populations at residual tumor lesions—obvious enhancement of antitumor-associated immune cell populations and antitumor cytokines, such as $CD8^+$T cells, $CD4^+$T cells, and M1-type macrophages, as well as TNF-α, IFN-γ, and IL-6. This study not only confirms that the control of ELE release kinetics can significantly affect postoperative recurrence and metastasis of breast cancer but also provides a viable strategy for postoperative treatment of other cancers using ELE drugs.

RESULTS AND DISCUSSION

Preparation and Characterization of ELE Nanodrug. Elemene (ELE) is a typical class of sesquiterpene hydrocarbons, showing strong hydrophobicity and moderate volatility.[30] The ELE injections that have been commercialized are formulated into a practicable drug through liposomal carriers;[31] however, the dynamic nature of liposomes is speculated to potentially lead to volatilization and loss of ELE.[32] Considering this problem, this work employed lipid−polymer hybrid nanoparticles (LPNPs)[33,34] with a more stable structure to encapsulate ELE, aiming to stabilize the loaded ELE. As depicted in Figure 1A, the ELE nanodrug (ELE@LPNPs) was prepared by utilizing biodegradable poly(lactic-*co*-glycolic acid) (PLGA) and amphiphilic polyethylene glycol (PEG)-modified distearoyl-phosphatidyl-ethanolamine (DSPE) (DSPE-PEG), in which the introduced polymer is expected to reduce the volatilization of ELE during subsequent operations. An orthogonal experimental design with three factors/three levels (Figure 1B) was employed to screen the optimal ELE@LPNP formulation. Figure 1C displays the encapsulation efficiency and drug-loading capacity of the nine ELE nanoformulations. Formulations 1−8 exhibited satisfactory ELE encapsulation efficiency, while formulation 9 showed the lowest encapsulation efficiency, possibly due to the lowest proportion of polymer in this formulation, thereby resulting in reduced ELE encapsulation. The sizes of these 9 ELE nanoformulations mostly ranged between 100 and 200 nm, with a surface zeta potential distribution between 0 and −50 mV (Figure 1D). Considering the requirements for nanomedicines in subsequent biomedical applications, including high encapsulation efficiency, drug-loading capacity, and small size, we selected formulation 6 as a representative ELE

https://doi.org/10.1021/jacs.4c12531
J. Am. Chem. Soc. XXXX, XXX, XXX−XXX

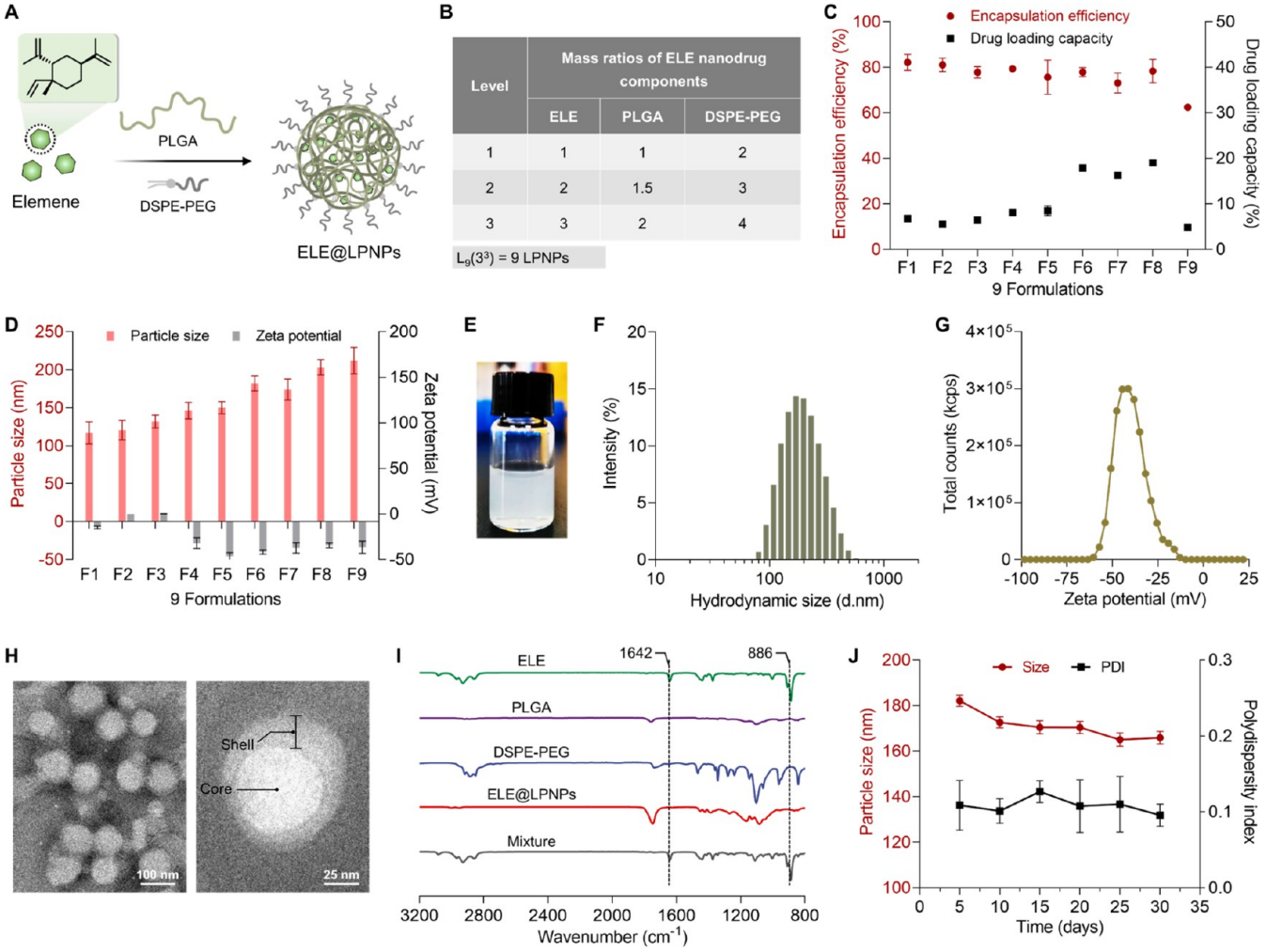

Figure 1. Preparation and characterization of the ELE nanodrug. (A) Schematic illustration of ELE@LPNP preparation. (B) Orthogonal experimental table for determining the optimal ELE@LPNP nanoformulation. (C) Encapsulation efficiency and drug-loading capacity of the 9 ELE@LPNP nanoformulations. (D) Particle sizes and zeta potentials of the 9 ELE@LPNP nanoformulations. (E) Photograph of a representative ELE@LPNP (F6) solution. (F) Hydrodynamic size and (G) zeta potential distribution of the ELE@LPNPs. (H) Representative TEM images of the ELE@LPNPs. (I) FTIR spectra of various substances. (J) Changes in particle size and polydispersity index during 1 month of storage at 37 °C.

nanodrug for further studies, and, for convenience, formulation 6 is referred to as ELE@LPNPs.

Figure 1E displays the ELE@LPNP solution, which exhibits a clear and faintly milky appearance. Dynamic light scattering (DLS) was used to characterize the size distribution of ELE@LPNPs (average size of 182 ± 3.42 nm, polydispersity index of 0.111, Figure 1F). Furthermore, the surface of ELE@LPNPs also possesses sufficient negative charge (average potential −41.82 ± 2.45 mV; Figure 1G) to support their colloidal stability in the solution. Transmission electron microscopy (TEM) revealed the microscopic morphology of ELE@LPNPs, which exhibited roughly spherical structures (Figure 1H); under higher magnifications; ELE@LPNPs displayed a distinct "core−shell" architecture. Fourier transform infrared spectroscopy further confirmed the encapsulation of ELE within LPNPs rather than existing in a free state; as shown in Figure 1I, the characteristic peaks of free ELE at 1642 and 886 cm^{-1} disappeared in ELE@LPNP samples, whereas these peaks were present in the simple mixtures of these substances.[35] Additionally, the size and PDI of ELE@LPNPs remained negligibly changed during 1 month of storage at 4 °C (Figure S1) and 37 °C (Figure 1J), demonstrating adequate colloidal stability. Taken together, these results demonstrate the successful preparation of ELE@LPNPs and their favorable physical properties for subsequent applications.

Preparation and Characterization of ELE@LPNPs@Gel. Previous reports have demonstrated that hydrogels can control drug release kinetics through swelling behavior, diffusion barriers, and degradation rate.[36−38] Therefore, a hydrogel system was selected for this purpose (Figure 2A). Hyaluronic acid (HA), an FDA-approved biopolymer naturally found in the body, possesses numerous desirable properties for biomedical applications, including excellent biocompatibility, versatility in adopting various physical forms, and the ability to control drug release in both spatial and temporal dimensions.[39,40] To further improve the mechanical properties and adhesive capability of the prepared hydrogel, dopamine (DA) was chemically conjugated onto the side chains of HA,[41,42] and the obtained DA-conjugated HA (HADA) is illustrated in Figure S2. HADAs with different DA grafting degrees (lower HADA-1 and higher HADA-2) were obtained by controlling the reaction molar ratio of HA to DA, which affects the subsequent gelation of HADA. The H^1 NMR spectra of HA, DA, and HADA shown in Figure 2B demonstrate that the

https://doi.org/10.1021/jacs.4c12531
J. Am. Chem. Soc. XXXX, XXX, XXX−XXX

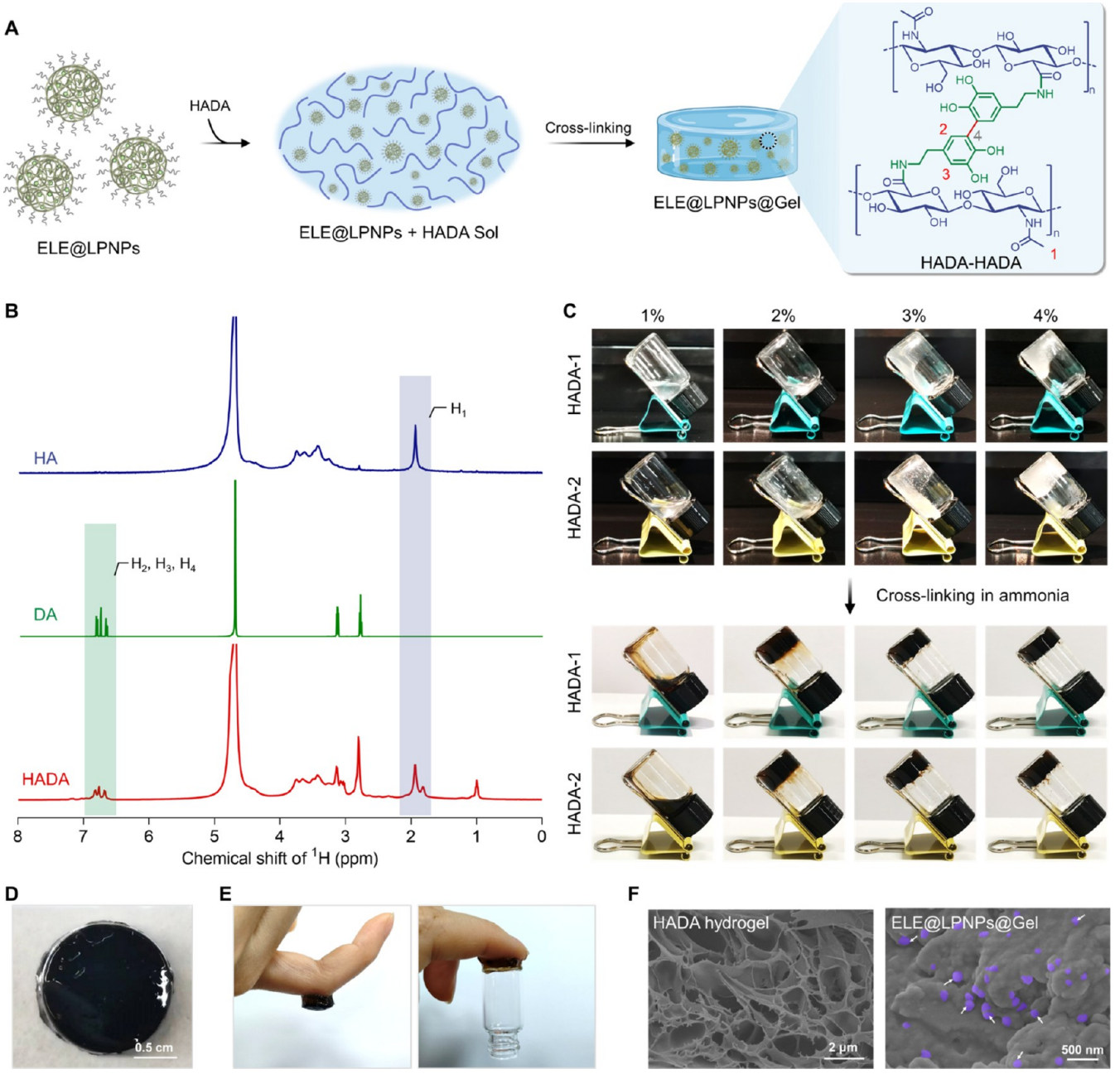

Figure 2. Preparation and characterization of ELE@LPNPs@Gel. (A) Schematic illustration of the preparation of ELE@LPNPs@Gel. (B) ^{1}H NMR spectra of HA, DA, and HADA. (C) Optimization of the HADA hydrogel at different gel concentrations and DA grafting degrees. (D) Photograph of ELE@LPNPs@Gel. (E) Photograph of the adhesion of ELE@LPNPs@Gel to the skin and glass. (F) SEM images of the blank HADA hydrogel and ELE@LPNPs@Gel. White arrows indicate loaded ELE@LPNPs.

characteristic peaks of DA at 6.7 ppm and HA at 2.0 ppm were both present in the spectrum of the purified HADA, confirming the successful synthesis of HADA, as also evidenced by Fourier transform infrared (FTIR) characterization (Figure S3).

The preparation of HADA hydrogels was optimized. Specifically, intermolecular cross-linking occurs between HADA molecules under the action of ammonia, resulting in the formation of a three-dimensional network structure, *i.e.*, a hydrogel. As shown in Figure 2C, HADA with different DA grafting degrees (HADA-1, HADA-2) formed more shaped and firm hydrogels with increasing gel concentration. Considering the need to achieve slow-release kinetics of the ELE nanodrug and implantable applications, a 4% concentration of HADA-2 with a high DA grafting degree was chosen for subsequent experiments, which are required to possess moderate mechanical properties and appropriate porosity. Figure 2D shows a photograph of the ELE@LPNP-loaded hydrogel (ELE@LPNPs@Gel) that exhibits a relatively stable shape. Due to the introduction of dopamine, the hydrogel also exhibits excellent bioadhesion (Figure 2E), which makes it a potential candidate for implantable hydrogel applications. The HADA hydrogel observed under scanning electron microscopy (SEM) displayed distinct voids and cross-linking structures; noticeable spherical structures were observed after loading ELE@LPNPs (Figure 2F), which were inferred to be ELE@

https://doi.org/10.1021/jacs.4c12531
J. Am. Chem. Soc. XXXX, XXX, XXX−XXX

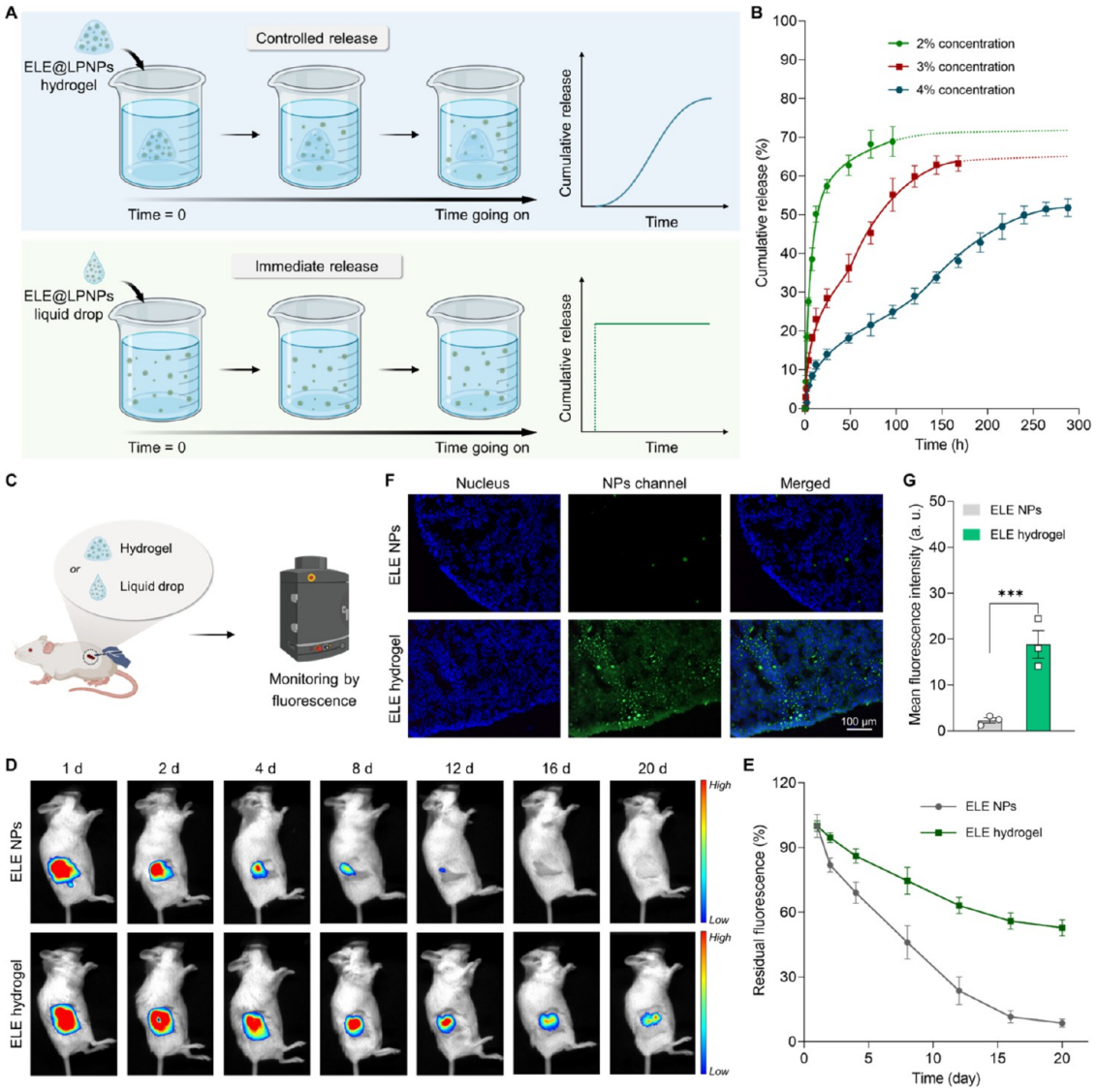

Figure 3. Release kinetic profiles of the ELE hydrogel *in vitro* and *in vivo*. (A) Schematic illustration of the release kinetics of ELE from different formulations. (B) *In vitro* release kinetic profiles of ELE from three ELE hydrogels. (C) Schematic illustration of the release behavior of the two ELE formulations at the mouse level. (D) Fluorescence IVIS imaging of mice implanted with the two ELE formulations on different days, with DiR as a fluorescent label. (E) The percentage of residual fluorescence quantified from the images in (D), normalized to the fluorescence intensity at the initial time. (F) Fluorescence images of the surrounding tumor tissues implanted with the two ELE formulations after 20 days, labeled with coumarin 6. (G) The mean fluorescence intensity quantified from the images in (F). A one-way ANOVA test was used to determine statistical significance. ***$P < 0.001$.

LPNPs. Moreover, ELE@LPNPs@Gel exhibited appropriate storage and loss moduli (Figure S4), excellent self-healing capabilities (Figure S5), and good mechanical properties under external strain forces (Figure S6). The soft and stretchable mechanical properties of the ELE hydrogel make it highly suitable for subcutaneous implantation applications.[43] The swelling ratio of the hydrogel is an indicator that affects the capacity and rate of drug release. ELE@LPNPs@Gel exhibited a swelling ratio of approximately 1.5 times its original weight (Figure S7), indicating its good potential for drug release. These results collectively indicate that ELE@LPNPs@Gel possesses outstanding mechanical properties and is suitable for subcutaneous implantable biomedical applications.

Release Kinetics Control of ELE Nanodrug by ELE@LPNP Hydrogel. The release kinetics of the drug can be controlled by the formulation design.[44] This work utilized the above-prepared hydrogel (see the Results and Discussion section) as an excipient to regulate the release kinetics of ELE. As illustrated in Figure 3A, when the prepared ELE@LPNP hydrogel is placed in a medium, the hydrogel undergoes swelling due to water absorption, causing the loosening of the diffusion barrier based on the polymeric three-dimensional network,[45] which allows the ELE@LPNPs loaded within the hydrogel to diffuse into the medium. Due to the presence of the diffusion barrier, the release rate of ELE@LPNPs from the hydrogel to the medium is slow, that is "controlled release". In contrast, when the ELE@LPNP liquid drop is directly added to the medium, they diffuse rapidly, that is "immediate release".

In this study, the diffusion barrier of the hydrogel was adjusted by changing the hydrogel concentration, which affects the mesh size of the hydrogel network, thereby regulating the diffusion rate of the loaded ELE@LPNPs, yielding three types

https://doi.org/10.1021/jacs.4c12531
J. Am. Chem. Soc. XXXX, XXX, XXX−XXX

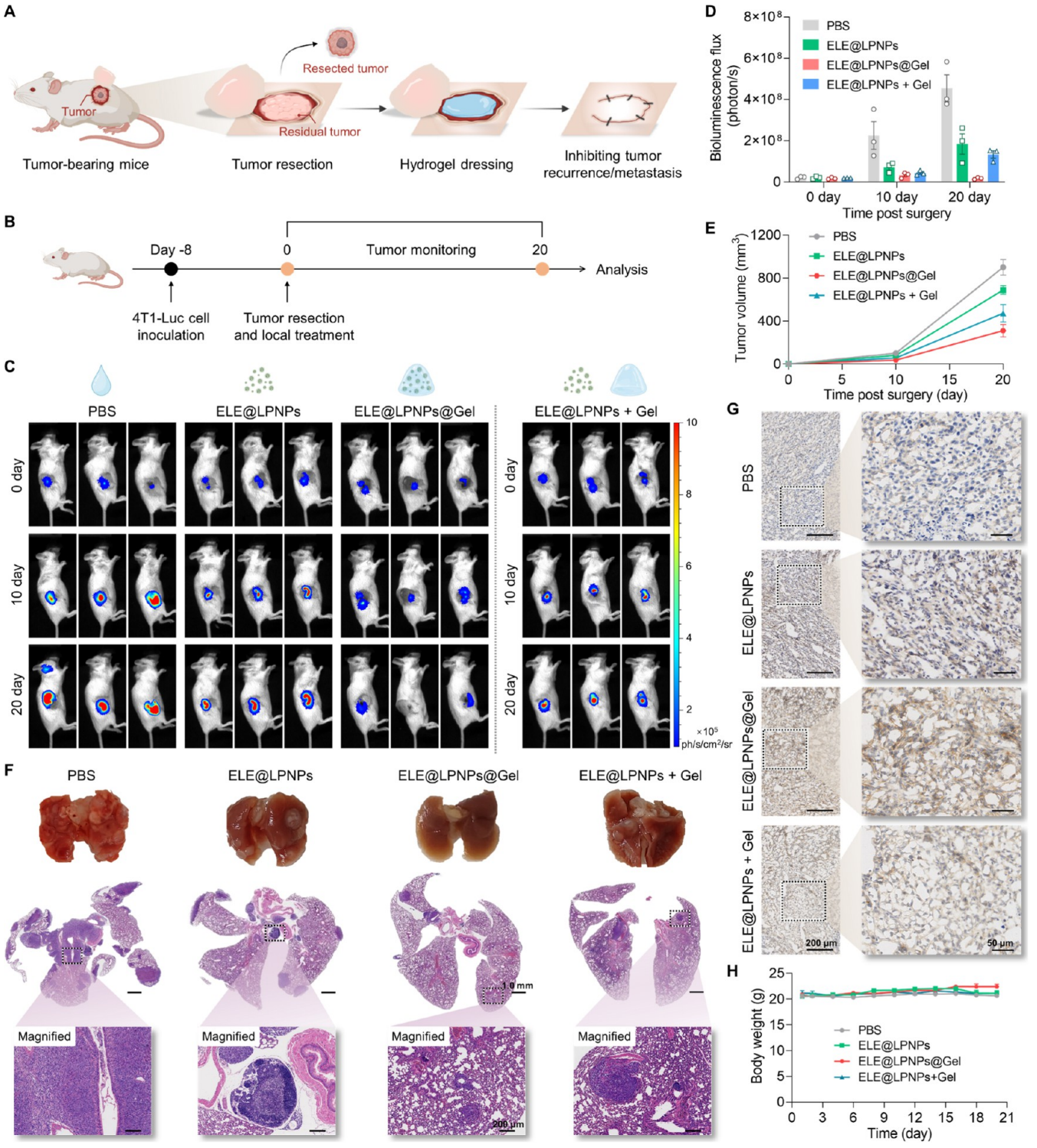

Figure 4. Efficacy of ELE@LPNPs@Gel in inhibiting tumor recurrence and metastasis *in vivo*. (A) Schematic illustration of the operation procedure of the hydrogel inhibiting tumor recurrence and metastasis. (B) Experimental timeline of treatment to inhibit tumor recurrence and metastasis. (C) *In vivo* bioluminescence imaging of 4T1-Luc tumor-bearing mice after different treatments. (D) Quantification of bioluminescence from the images in (C). (E) Changes in the tumor volume after the different treatments. (F) Representative photographs of lung tissue from mice and their corresponding H&E stained images after different treatments. (G) Representative immunohistochemical staining images of E-cadherin in residual tumor tissues after different treatments. (H) Changes in the body weight of mice after different treatments.

of hydrogels with distinct release kinetics of ELE nanodrugs (Figure 3B). The 2% concentration hydrogel released ELE@LPNPs at the fastest rate, releasing about 68% of the initial amount on the fourth day. The 3% concentration hydrogel reached the release endpoint on the seventh day, and the final release percentage of ELE@LPNPs was about 63%. The 4% concentration hydrogel released the slowest among the three hydrogels, reaching the release endpoint on the 11th day, and the cumulative release percentage of ELE@LPNPs was about 52%.

https://doi.org/10.1021/jacs.4c12531
J. Am. Chem. Soc. XXXX, XXX, XXX−XXX

Furthermore, the sustained release behavior of the ELE hydrogel with slow-release kinetics (the 4% concentration hydrogel) at the mouse level was investigated (Figure 3C), with a coloaded near-infrared fluorescent dye DiR as a label. ELE in the hydrogel form remained at the subcutaneous implant site for up to 20 days, exhibiting an obvious signal intensity (bottom panel in Figure 3D). In contrast, ELE nanoparticles (ELE@LPNPs) could only be maintained until day 12, with signal intensity dropping to undetectable levels (top panel in Figure 3D). Figure 3E shows the quantitative results of the residual signal from Figure 3D, indicating that on day 20, over 50% of the ELE remained, which demonstrates its excellent sustained drug release capability. To more accurately compare the differences in the effects of the release kinetics, fluorescence histology was utilized. ELE nanoparticles and ELE hydrogel (coloaded with green fluorescent dye coumarin 6 as a label) were implanted subcutaneously in mice. After 20 days, fluorescence histology was conducted on the tumor tissues at the implantation sites. As shown in Figure 3F, for the ELE NPs droplet group, almost no ELE nanoparticles were observed in the tissue at the implantation site (green channel), whereas for the ELE hydrogel group, significant fluorescence signals were still clearly observed in the tissue at the implantation site, indicating a high abundance of ELE nanoparticles in the surrounding tissues. Quantification of the fluorescence histology in Figure 3G also confirmed significant differences between the two groups.

ELE@LPNP Hydrogel with Slow-Release Kinetics Significantly Inhibits Tumor Recurrence and Metastasis. Elemene, an active ingredient extracted from plants, has been verified to exhibit excellent antitumor efficacy. In this work, we examined the efficacy of the ELE hydrogel with slow-release kinetics in preventing tumor recurrence and metastasis postsurgery (Figure 4A), using 4T1 breast cancer as the model.

Specifically, as depicted in Figure 4B, luciferase-labeled 4T1 cells were subcutaneously inoculated into Balb/c mice; after 8 days, the majority of the tumor was surgically resected, leaving a small residual portion to simulate the postsurgery tumor residue in clinical practice. Subsequently, local administration of different ELE formulations was performed at the residual tumor sites, and the growth of the remaining tumors was monitored. After the three treatments, the tumor recurrence in the three groups was 25-fold (PBS), 8.6-fold (ELE@LPNPs), and 1.0-fold (ELE@LPNPs@Gel), respectively, with the bioluminescence flux on day 0 as the initial standard, as shown in Figures 4C−E and S8A. The enhanced inhibition of tumor recurrence by the ELE hydrogel was further evidenced by the tumor recurrence inhibition ratio: 65.5% inhibition for the ELE@LPNP droplets and 96% inhibition for the ELE@LPNPs@Gel hydrogel (Figure S8B). These results demonstrate the significant and potent efficacy of the ELE hydrogel in inhibiting tumor recurrence.

To exclude the influence of the hydrogel itself on the antitumor recurrence effect, a control group ("ELE@LPNPs + Gel" group in Figure 4C−E) was set up where the ELE@LPNP droplets and HADA hydrogel were jointly administered in separate forms; the results showed similar antitumor recurrence efficacy to that of administering ELE@LPNPs alone, indicating that the enhanced antitumor recurrence capability was not due to the hydrogel itself but rather the altered release kinetics of ELE@LPNPs.

Furthermore, the efficacy of the ELE@LPNPs@Gel hydrogel in inhibiting tumor metastasis was also examined. As shown in Figure 4F, the lung tissues of the PBS control group exhibited numerous tumor-like metastases. Compared with ELE@LPNPs droplets, ELE@LPNPs@Gel significantly inhibited lung metastasis from breast cancer (Figure S9) and the expression level of Ki67 (Figure S10). The high expression of E-cadherin, a marker associated with inhibiting cancer metastasis,[46] in residual tumor tissues, further confirmed the enhanced efficacy of ELE@LPNPs@Gel in inhibiting tumor metastasis compared with ELE@LPNPs (Figure 4G). Collectively, these findings demonstrate that the ELE@LPNP hydrogel with slow-release kinetics significantly inhibited tumor recurrence and metastasis rather than any additional effects of the hydrogel itself. Additionally, there was no obvious decrease in the body weight of the mice during the treatment period, indicating the good biocompatibility of ELE@LPNPs@Gel (Figure 4H).

In addition, the *in vivo* safety of ELE@LPNPs@Gel was further evaluated. First, a hemolysis test was used to assess the hemocompatibility of ELE@LPNPs@Gel. As shown in Figure S11, ELE@LPNPs@Gel exhibited negligible hemolysis, with a hemolysis rate of 3.5%. Moreover, the safety of extracting the solution of ELE@LPNPs@Gel was evaluated according to a previous study.[47] When different concentrations of extracting solution of ELE@LPNPs@Gel (62.5−500 μg mL^{-1}) were coincubated with L929 cells for 24 h, the cell viability showed no significant change compared with the control group (Figure S12). Furthermore, after ELE@LPNPs@Gel was implanted into healthy mice for 30 days, the blood biochemical parameters in blood samples were determined and major organs were collected for hematoxylin-eosin staining. Compared with normal healthy mice, ELE@LPNPs@Gel treatment had no significant effect on the blood (Figure S13) or organs (Figure S14) of the mice. These results demonstrated that ELE@LPNPs@Gel possesses good biosafety.

ELE@LPNP Hydrogel with Slow-Release Kinetics Induces Enhanced Antitumor Immune Response *In Vivo*. Furthermore, the cytotoxicity of ELE@LPNPs on 4T1 and MDA-MB-231 cells was measured, and ELE@LPNPs exhibited a stronger cell-kill effect than free ELE (Figure S15). This was confirmed by the pro-apoptic effect of ELE@LPNPs on 4T1; the apoptosis rate of ELE@LPNPs on 4T1 cells was approximately 2.3 times that of free ELE (Figure S16). We also investigated the differences in the uptake of ELE@LPNPs and free ELE in the two cancer cell lines. The results showed that compared with free ELE, ELE@LPNPs were easily internalized by cells. Therefore, ELE@LPNPs had more obvious cytotoxicity in the two cancer cell lines (Figures S17 and S18).

A previous study from our group demonstrated the efficacy of elemene in inducing immune responses.[15] Therefore, here, the capability of the ELE@LPNP hydrogel with slow-release kinetics in inducing antitumor immune responses was investigated. Due to the primary role of T cells and macrophages in antitumor immunity,[48−50] their cell populations in residual tumor tissues were analyzed by flow cytometry 20 days after different treatments (Figures S19 and S20). As shown in Figure S21, compared with ELE@LPNPs, the treatment with ELE@LPNPs@Gel increased the population of CD45$^+$ cells within residual tumor tissues, including myeloid and lymphoid immune cells, which provided the cell prerequisites for enhanced antitumor immunity. As T cells activated by antigen-presenting cells play a crucial role in inducing adaptive antitumor immunity, the population of T cells within residual tumors was further analyzed. Specifically,

https://doi.org/10.1021/jacs.4c12531
J. Am. Chem. Soc. XXXX, XXX, XXX−XXX

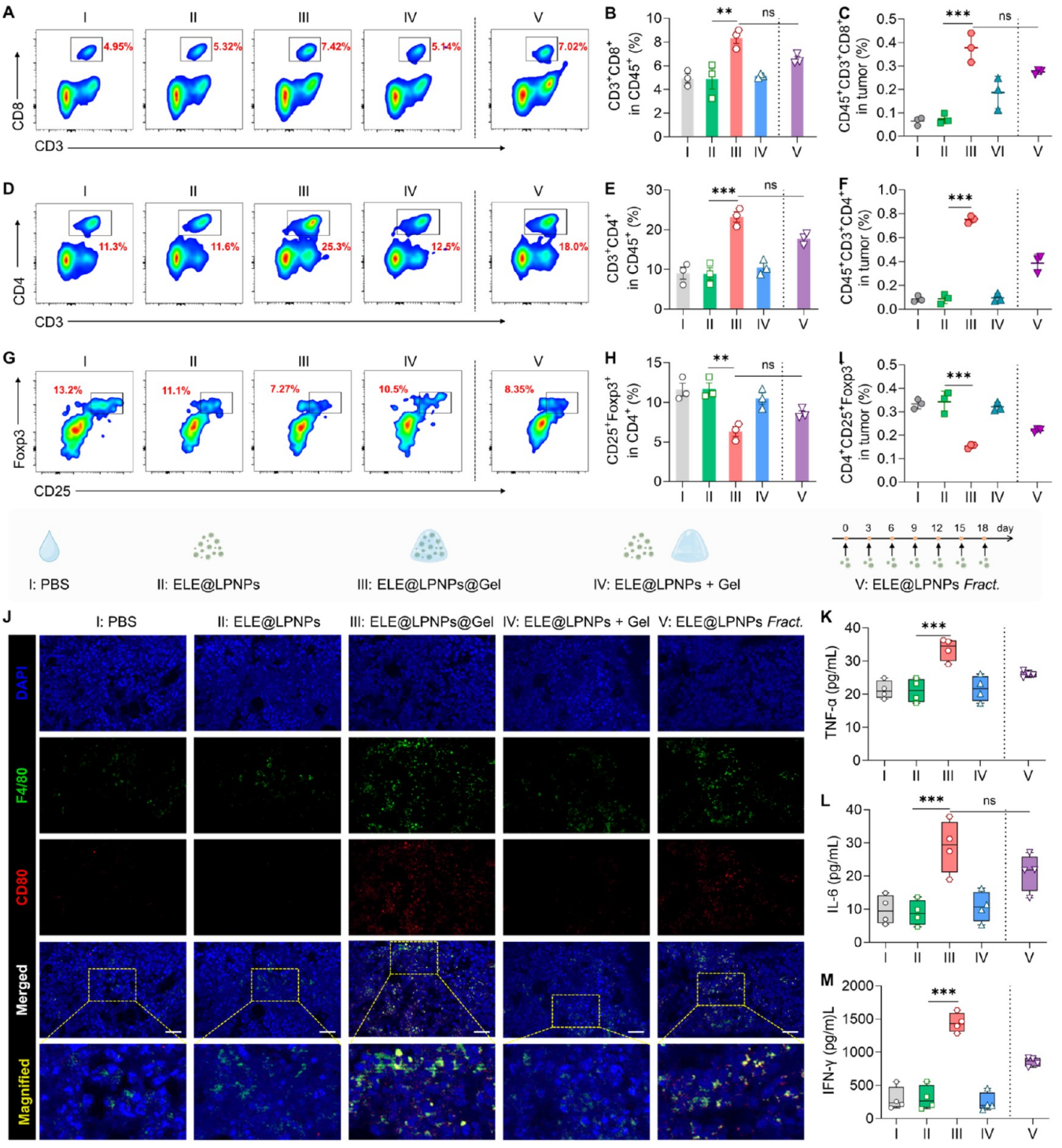

Figure 5. Antitumor immune response after treatment with different ELE nanoformulations. (A) Representative flow cytometric analysis of $CD3^+CD8^+$ T cells after various treatments, (B) quantification of the percentage of $CD3^+CD8^+$ cells in $CD45^+$ cells, and (C) quantification of the percentage of $CD45^+CD3^+CD8^+$ cells in tumor cells. (D) Representative flow cytometric analysis of $CD3^+CD4^+$ T cells after various treatments, (E) quantification of the percentage of $CD3^+CD4^+$ cells in $CD45^+$ cells, and (F) quantification of the percentage of $CD45^+CD3^+CD4^+$ cells in tumor cells. (G) Representative flow cytometric analysis of $CD25^+Foxp3^+$ T cells after various treatments, (H) quantification of the percentage of $CD25^+Foxp3^+$ cells in $CD4^+$ cells, and (I) quantification of the percentage of $CD25^+Foxp3^+$ cells in tumor cells. (J) Immunofluorescence images of residual tumor tissues following different treatments. Green: F4/80 antibody staining for macrophages, red: CD80 antibody staining for M1-type macrophages, and blue: DAPI staining for cell nuclei. Scale bars are 40 μm. Secretion levels of proinflammatory cytokines: (K) TNF-α, (L) IL-6, and (M) IFN-γ in the serum of mice. The data represent the mean ± SD. A one-way ANOVA test was used to determine statistical significance. *P < 0.05, **P < 0.01, and ***P < 0.001.

the population of cytotoxic T cells ($CD8^+$ cells) within the residual tumors significantly increased after ELE@LPNPs@Gel treatment (Figure 5A−C), which was 4.2-fold higher than that after ELE@LPNPs treatment (Figure 5C). $CD4^+$ cells, a type of helper T cells, concurrently showed increased populations after ELE@LPNPs@Gel treatment (Figure 5D−

https://doi.org/10.1021/jacs.4c12531
J. Am. Chem. Soc. XXXX, XXX, XXX−XXX

F), a 7.5-fold increase compared with the ELE@LPNPs treatment (Figure 5F). Additionally, regulatory T cells, a type of immunosuppressive immune cell, exhibited a substantial reduction in population after ELE@LPNPs@Gel treatment (Figure 5G−I), a 55% decrease in contrast to the ELE@LPNP group (Figure 5I).

M1-type macrophages, a type of tumor-associated macrophage, play a proinflammatory role in antitumor immunity, and their increased population is beneficial for further clearance of residual tumors postsurgery.[51,52] Here, the abundance of M1-type macrophages in residual tumor tissues after different treatments was observed using immunofluorescence imaging. As shown in Figure 5J, the residual tumor tissues treated with ELE@LPNPs@Gel (Group III) exhibited prominent green (labeled F4/80) and red fluorescence (labeled CD80), which merged into yellow fluorescence (labeled M1-type macrophages), indicating the enhanced abundance of M1-type macrophages compared with the ELE@LPNP treatment (Group II).

Moreover, the proinflammatory cytokines in the serum were determined using the ELISA method. Treatment with ELE@LPNPs@Gel significantly increased the production of proinflammatory cytokines (Figure 5K−M), including TNF-α, IL-6, and IFN-γ in serum compared with the ELE@LPNP treatment. The above results collectively demonstrate that ELE@LPNPs@Gel promoted an antitumor immune response in comparison to ELE@LPNPs. The "ELE@LPNPs + Gel" group exhibited similar results to the ELE@LPNPs group (Figure 5A−M), which rules out the impact of the hydrogel itself on the antitumor immune response. In addition, to positively prove that the different immune effects are attributed to the difference in the release kinetics of elemene, an additional positive control group was set up, wherein a single dose of ELE@LPNPs was divided into seven fractions and administered every 3 days (*i.e.*, ELE@LPNP fractionation, as illustrated in the middle panel in Figure 5) to simulate the slow-release kinetics of elemene. The results were consistent with ELE@LPNPs@Gel in regulating T cells and macrophages as well as modulating various proinflammatory cytokines in the serum, which positively provides further evidence that the enhanced immune effects are indeed attributed to the slow-release kinetics of elemene. Overall, the mechanisms by which ELE hydrogels exhibit enhanced antitumor immunity can be attributed to the following reasons: (1) ELE induces immunogenic cell death in tumor cells, triggering downstream immune responses and releasing tumor antigens.[53] (2) ELE promotes the polarization of macrophages from M2 to the M1 phenotype through the ROS-induced NF-κB-TNF-α-iNOS signaling pathway,[15] and the activated M1 macrophages facilitate antitumor immunity; and (3) the ELE hydrogel imparts sustained release properties to ELE, significantly extending its pharmacological effects, including immunoactivity. These properties maximize the effect of the ELE hydrogel in modulating tumor immunity.

CONCLUSIONS

In summary, this study successfully developed a novel ELE formulation, ELE hydrogel (ELE@LPNPs@Gel), which demonstrated controlled-release kinetics of ELE, and significantly inhibited breast cancer recurrence and metastasis in preclinical models compared with ELE nanodrug droplets. More importantly, this novel ELE hydrogel significantly altered the immune microenvironment at the lesion sites, augmenting the populations of antitumor immune cells and cytokines. The findings underscore the potential of the ELE hydrogel in inhibiting postoperative cancer recurrence and metastases by prolonging drug exposure and enhancing antitumor immune responses. Overall, the work presented herein advances the understanding of drug delivery systems and also highlights the tremendous potential of combining TCM with modern pharmaceutical technologies.

Although the current research offers compelling evidence of hydrogel efficacy in preclinical models, further studies are needed to evaluate its effectiveness across a broader range of tumor models. Expanding our investigation to include diverse cancer types and larger animal models would enhance the generalizability of these findings. Additionally, future research should focus on uncovering the precise mechanisms through which ELE modulates the immune microenvironment, as this could help identify new therapeutic targets and provide deeper insights into the role of ELE in immune response modulation. Optimizing the hydrogel formulation for various clinical applications is also a key area of future exploration.

ASSOCIATED CONTENT

Supporting Information

The Supporting Information is available free of charge at https://pubs.acs.org/doi/10.1021/jacs.4c12531.

Experimental details and characterization data including chemicals and materials; synthesis and characterization of HADA; construction of the ELE@LPNPs and ELE@LPNPs@Gel; general physicochemical characterization, mechanical testing, and swelling behavior of ELE@LPNPs@Gel; *in vitro* ELE release; cell culture, cellular internalization, cytotoxicity, and pro-apoptotic effects of ELE@LPNPs on tumor cells; *in vivo* postsurgical tumor recurrence inhibition, antitumor immunity, and hemolysis tests; safety evaluation of ELE@LPNPs@Gel; statistical analysis (Figures S1−S21); and orthogonal experiments table of ELE@LPNP preparation (PDF)

AUTHOR INFORMATION

Corresponding Authors

Wei Tao − *Center for Nanomedicine and Department of Anesthesiology, Brigham and Women's Hospital, Harvard Medical School, Boston, Massachusetts 02115, United States;* orcid.org/0000-0002-4277-3728; Email: wtao@bwh.harvard.edu

Na Kong − *Liangzhu Laboratory, Zhejiang University, Hangzhou, Zhejiang 311121, China; Center for Nanomedicine and Department of Anesthesiology, Brigham and Women's Hospital, Harvard Medical School, Boston, Massachusetts 02115, United States;* orcid.org/0000-0002-3823-8335; Email: kongna@zju.edu.cn

Tian Xie − *School of Pharmacy; Key Laboratory of Elemene Class Anti-Cancer Chinese Medicines; Engineering Laboratory of Development and Application of Traditional Chinese Medicines; Collaborative Innovation Center of Traditional Chinese Medicines of Zhejiang Province, Hangzhou Normal University, Hangzhou, Zhejiang 311121, China; State Key Laboratory of Southwestern Chinese Medicine Resources, School of Pharmacy, Chengdu University of Traditional Chinese Medicine, Chengdu, Sichuan 611137, China*; Email: tianxie@hznu.edu.cn

https://doi.org/10.1021/jacs.4c12531
J. Am. Chem. Soc. XXXX, XXX, XXX−XXX

Authors

Jing Xian − *School of Pharmacy; Key Laboratory of Elemene Class Anti-Cancer Chinese Medicines; Engineering Laboratory of Development and Application of Traditional Chinese Medicines; Collaborative Innovation Center of Traditional Chinese Medicines of Zhejiang Province, Hangzhou Normal University, Hangzhou, Zhejiang 311121, China; State Key Laboratory of Southwestern Chinese Medicine Resources, School of Pharmacy, Chengdu University of Traditional Chinese Medicine, Chengdu, Sichuan 611137, China; Liangzhu Laboratory, Zhejiang University, Hangzhou, Zhejiang 311121, China*

Fan Xiao − *Liangzhu Laboratory, Zhejiang University, Hangzhou, Zhejiang 311121, China; Center for Nanomedicine and Department of Anesthesiology, Brigham and Women's Hospital, Harvard Medical School, Boston, Massachusetts 02115, United States;* orcid.org/0000-0003-3429-5241

Jianhua Zou − *School of Pharmacy; Key Laboratory of Elemene Class Anti-Cancer Chinese Medicines; Engineering Laboratory of Development and Application of Traditional Chinese Medicines; Collaborative Innovation Center of Traditional Chinese Medicines of Zhejiang Province, Hangzhou Normal University, Hangzhou, Zhejiang 311121, China*

Wei Luo − *School of Pharmacy; Key Laboratory of Elemene Class Anti-Cancer Chinese Medicines; Engineering Laboratory of Development and Application of Traditional Chinese Medicines; Collaborative Innovation Center of Traditional Chinese Medicines of Zhejiang Province, Hangzhou Normal University, Hangzhou, Zhejiang 311121, China;* orcid.org/0000-0001-6012-0758

Shiqi Han − *School of Pharmacy; Key Laboratory of Elemene Class Anti-Cancer Chinese Medicines; Engineering Laboratory of Development and Application of Traditional Chinese Medicines; Collaborative Innovation Center of Traditional Chinese Medicines of Zhejiang Province, Hangzhou Normal University, Hangzhou, Zhejiang 311121, China*

Ziwei Liu − *Liangzhu Laboratory, Zhejiang University, Hangzhou, Zhejiang 311121, China*

Yiquan Chen − *Liangzhu Laboratory, Zhejiang University, Hangzhou, Zhejiang 311121, China*

Qianru Zhu − *School of Pharmacy; Key Laboratory of Elemene Class Anti-Cancer Chinese Medicines; Engineering Laboratory of Development and Application of Traditional Chinese Medicines; Collaborative Innovation Center of Traditional Chinese Medicines of Zhejiang Province, Hangzhou Normal University, Hangzhou, Zhejiang 311121, China*

Meng Li − *School of Pharmacy; Key Laboratory of Elemene Class Anti-Cancer Chinese Medicines; Engineering Laboratory of Development and Application of Traditional Chinese Medicines; Collaborative Innovation Center of Traditional Chinese Medicines of Zhejiang Province, Hangzhou Normal University, Hangzhou, Zhejiang 311121, China*

Chuao Yu − *School of Pharmacy; Key Laboratory of Elemene Class Anti-Cancer Chinese Medicines; Engineering Laboratory of Development and Application of Traditional Chinese Medicines; Collaborative Innovation Center of Traditional Chinese Medicines of Zhejiang Province, Hangzhou Normal University, Hangzhou, Zhejiang 311121, China*

Qimanguli Saiding − *Center for Nanomedicine and Department of Anesthesiology, Brigham and Women's Hospital, Harvard Medical School, Boston, Massachusetts 02115, United States;* orcid.org/0000-0003-2783-5991

Complete contact information is available at: https://pubs.acs.org/10.1021/jacs.4c12531

Author Contributions

[⊥]J.X. and F.X. contributed equally to this work.

Notes

The authors disclose the following competing financial interests: They have applied for a patent related to this strategy.

The authors declare no competing financial interest.

■ ACKNOWLEDGMENTS

This work is supported by the Key Project of Zhejiang Ministry of Science and Technology (2021C03087 for T.X.), the National Natural Science Foundation of China (82122076 for N.K.), the China Postdoctoral Science Foundation (2023M733022 for F.X.), and the China Postdoctoral Fellowship Program of CPSF (GZB20230652 for F.X.). The authors thank Bin Xu for the assistance and the technical support by the Core Facilities, Liangzhu Laboratory, Zhejiang University. Schemes were created with BioRender.com.

■ REFERENCES

(1) Gan, X.; Shu, Z.; Wang, X.; Yan, D.; Li, J.; Ofaim, S.; Albert, R.; Li, X.; Liu, B.; Zhou, X.; Barabasi, A. L. Network medicine framework reveals generic herb-symptom effectiveness of traditional Chinese medicine. *Sci. Adv.* **2023**, *9* (43), No. eadh0215.

(2) Yang, Y.; Li, X.; Chen, G.; Xian, Y.; Zhang, H.; Wu, Y.; Yang, Y.; Wu, J.; Wang, C.; He, S.; Wang, Z.; Wang, Y.; Wang, Z.; Liu, H.; Wang, X.; Zhang, M.; Zhang, J.; Li, J.; An, T.; Guan, H.; Li, L.; Shang, M.; Yao, C.; Han, Y.; Zhang, B.; Gao, R.; Peterson, E. D.; CTS-AMI Investigators. Traditional Chinese medicine compound (Tongxinluo) and clinical outcomes of patients with acute myocardial infarction: The CTS-AMI randomized clinical trial. *J. Am. Med. Assoc.* **2023**, *330* (16), 1534−1545.

(3) Tu, Y. Artemisinin-a gift from traditional Chinese medicine to the world (Nobel Lecture). *Angew. Chem., Int. Ed.* **2016**, *55* (35), 10210−10226.

(4) Wang, J.; Xu, C.; Liao, F. L.; Jiang, T.; Krishna, S.; Tu, Y. A temporizing solution to ″artemisinin resistance″. *N. Engl. J. Med.* **2019**, *380* (22), 2087−2089.

(5) Xie, T. *Elemene Antitumor Drugs, Molecular Compatibility Theory and Its Applications in New Drug Development and Clinical Practice*; Elsevier: Cambridge, MA, USA, 2023.

(6) Hou, S.; Li, Z.; Chen, X.; Wang, W.; Duan, T.; Scampavia, L.; Yuan, Y.; Spicer, T. P.; Chen, X.; Xie, T. Elemene sensitizes pancreatic cancer cells to bortezomib by enhancing proteasome inhibition via molecular patch mechanism. *Signal Transduction Targeted Ther.* **2023**, *8* (1), No. 87.

(7) Chen, W.; Liu, C.; Ji, X.; Joseph, J.; Tang, Z.; Ouyang, J.; Xiao, Y.; Kong, N.; Joshi, N.; Farokhzad, O. C.; Tao, W.; Xie, T. Stanene-based nanosheets for β-elemene delivery and ultrasound-mediated combination cancer therapy. *Angew. Chem., Int. Ed.* **2021**, *60* (13), 7155−7164.

(8) Ji, X.; Tang, Z.; Liu, H.; Kang, Y.; Chen, L.; Dong, J.; Chen, W.; Kong, N.; Tao, W.; Xie, T. Nanoheterojunction-mediated thermoelectric strategy for cancer surgical adjuvant treatment and β-elemene combination therapy. *Adv. Mater.* **2023**, *35* (8), No. e2207391.

(9) Chen, P.; Li, X.; Zhang, R.; Liu, S.; Xiang, Y.; Zhang, M.; Chen, X.; Pan, T.; Yan, L.; Feng, J.; Duan, T.; Wang, D.; Chen, B.; Jin, T.; Wang, W.; Chen, L.; Huang, X.; Zhang, W.; Sun, Y.; Li, G.; Kong, L.; Chen, X.; Li, Y.; Yang, Z.; Zhang, Q.; Zhuo, L.; Sui, X.; Xie, T. Combinative treatment of β-elemene and cetuximab is sensitive to KRAS mutant colorectal cancer cells by inducing ferroptosis and inhibiting epithelial-mesenchymal transformation. *Theranostics* **2020**, *10* (11), 5107−5119.
(10) Liu, C.; Sun, S.; Feng, Q.; Wu, G.; Wu, Y.; Kong, N.; Yu, Z.; Yao, J.; Zhang, X.; Chen, W.; Tang, Z.; Xiao, Y.; Huang, X.; Lv, A.; Yao, C.; Cheng, H.; Wu, A.; Xie, T.; Tao, W. Arsenene nanodots with selective killing effects and their low-dose combination with β-elemene for cancer therapy. *Adv. Mater.* **2021**, *33* (37), No. e2102054.
(11) Feng, C.; Ouyang, J.; Tang, Z.; Kong, N.; Liu, Y.; Fu, L.; Ji, X.; Xie, T.; Farokhzad, O. C.; Tao, W. Germanene-based theranostic materials for surgical adjuvant treatment: Inhibiting tumor recurrence and wound infection. *Matter* **2020**, *3* (1), 127−144.
(12) Li, J.; Zeng, H.; You, Y.; Wang, R.; Tan, T.; Wang, W.; Yin, L.; Zeng, Z.; Zeng, Y.; Xie, T. Active targeting of orthotopic glioma using biomimetic liposomes co-loaded elemene and cabazitaxel modified by transferritin. *J. Nanobiotechnol.* **2021**, *19* (1), No. 289.
(13) Luo, L.; Zhou, J.; Liu, X.; Chen, Y.; Du, X.; Gao, L.; Sun, Y.; Wang, S. Development of modern Chinese medicine guided by molecular compatibility theory. *J. Adv. Res.* **2024**, DOI: 10.1016/j.jare.2024.08.005.
(14) Kong, N.; Zhang, R.; Wu, G.; Sui, X.; Wang, J.; Kim, N. Y.; Blake, S.; De, D.; Xie, T.; Cao, Y.; Tao, W. Intravesical delivery of KDM6A-mRNA via mucoadhesive nanoparticles inhibits the metastasis of bladder cancer. *Proc. Natl. Acad. Sci. U.S.A.* **2022**, *119* (7), No. e2112696119.
(15) Chen, W.; Li, Y.; Liu, C.; Kang, Y.; Qin, D.; Chen, S.; Zhou, J.; Liu, H. J.; Ferdows, B. E.; Patel, D. N.; Huang, X.; Koo, S.; Kong, N.; Ji, X.; Cao, Y.; Tao, W.; Xie, T. In situ engineering of tumor-associated macrophages via a nanodrug-delivering-drug (β-elemene@stanene) strategy for enhanced cancer chemo-immunotherapy. *Angew. Chem., Int. Ed.* **2023**, *62* (41), No. 202308413.
(16) Laracuente, M. L.; Yu, M. H.; McHugh, K. J. Zero-order drug delivery: State of the art and future prospects. *J. Controlled Release* **2020**, *327*, 834−856.
(17) Chen, Y. C.; Shishikura, S.; Moseson, D. E.; Ignatovich, A. J.; Lomeo, J.; Zhu, A.; Horava, S. D.; Richard, C. A.; Park, K.; Yeo, Y. Control of drug release kinetics from hot-melt extruded drug-loaded polycaprolactone matrices. *J. Controlled Release* **2023**, *359*, 373−383.
(18) Sethi, M.; Sukumar, R.; Karve, S.; Werner, M. E.; Wang, E. C.; Moore, D. T.; Kowalczyk, S. R.; Zhang, L.; Wang, A. Z. Effect of drug release kinetics on nanoparticle therapeutic efficacy and toxicity. *Nanoscale* **2014**, *6* (4), 2321−2327.
(19) Antimisiaris, S. G.; Marazioti, A.; Kannavou, M.; Natsaridis, E.; Gkartziou, F.; Kogkos, G.; Mourtas, S. Overcoming barriers by local drug delivery with liposomes. *Adv. Drug Delivery Rev.* **2021**, *174*, 53−86.
(20) Mikhail, A. S.; Morhard, R.; Mauda-Havakuk, M.; Kassin, M.; Arrichiello, A.; Wood, B. J. Hydrogel drug delivery systems for minimally invasive local immunotherapy of cancer. *Adv. Drug Delivery Rev.* **2023**, *202*, No. 115083.
(21) Wang, F.; Huang, Q.; Su, H.; Sun, M.; Wang, Z.; Chen, Z.; Zheng, M.; Chakroun, R. W.; Monroe, M. K.; Chen, D.; Wang, Z.; Gorelick, N.; Serra, R.; Wang, H.; Guan, Y.; Suk, J. S.; Tyler, B.; Brem, H.; Hanes, J.; Cui, H. Self-assembling paclitaxel-mediated stimulation of tumor-associated macrophages for postoperative treatment of glioblastoma. *Proc. Natl. Acad. Sci. U.S.A.* **2023**, *120* (18), No. e2204621120.
(22) Park, C. G.; Hartl, C. A.; Schmid, D.; Carmona, E. M.; Kim, H. J.; Goldberg, M. S. Extended release of perioperative immunotherapy prevents tumor recurrence and eliminates metastases. *Sci. Transl. Med.* **2018**, *10* (433), No. eaar1916, DOI: 10.1126/scitranslmed.aar1916.
(23) Xu, X.; Gu, Z.; Chen, X.; Shi, C.; Liu, C.; Liu, M.; Wang, L.; Sun, M.; Zhang, K.; Liu, Q.; Shen, Y.; Lin, C.; Yang, B.; Sun, H. An injectable and thermosensitive hydrogel: Promoting periodontal regeneration by controlled-release of aspirin and erythropoietin. *Acta Biomater.* **2019**, *86*, 235−246.
(24) Tan, J.; Zhang, M.; Hai, Z.; Wu, C.; Lin, J.; Kuang, W.; Tang, H.; Huang, Y.; Chen, X.; Liang, G. Sustained release of two bioactive factors from supramolecular hydrogel promotes periodontal bone regeneration. *ACS Nano* **2019**, *13* (5), 5616−5622.
(25) Armaly, M. F.; Rao, K. R. The effect of pilocarpine ocusert with different release rates on ocular pressure. *Invest. Ophthalmol. Visual Sci.* **1973**, *12* (7), 491−496.
(26) Weiser, J. R.; Saltzman, W. M. Controlled release for local delivery of drugs: Barriers and models. *J. Controlled Release* **2014**, *190*, 664−673.
(27) Kim, J.; Archer, P. A.; Manspeaker, M. P.; Avecilla, A. R. C.; Pollack, B. P.; Thomas, S. N. Sustained release hydrogel for durable locoregional chemoimmunotherapy for BRAF-mutated melanoma. *J. Controlled Release* **2023**, *357*, 655−668.
(28) Kang, T.; Cha, G. D.; Park, O. K.; Cho, H. R.; Kim, M.; Lee, J.; Kim, D.; Lee, B.; Chu, J.; Koo, S.; Hyeon, T.; Kim, D.-H.; Choi, S. H. Penetrative and sustained drug delivery using injectable hydrogel nanocomposites for postsurgical brain tumor treatment. *ACS Nano* **2023**, *17* (6), 5435−5447.
(29) Park, S. H.; Kim, R. S.; Stiles, W. R.; Jo, M.; Zeng, L.; Rho, S.; Baek, Y.; Kim, J.; Kim, M. S.; Kang, H.; Choi, H. S. Injectable thermosensitive hydrogels for a sustained release of iron nanochelators. *Adv. Sci.* **2022**, *9* (15), No. e2200872.
(30) Tian, H.; Zhao, F.; Qi, Q. R.; Yue, B. S.; Zhai, B. T. Targeted drug delivery systems for elemene in cancer therapy: The story thus far. *Biomed. Pharmacother.* **2023**, *166*, No. 115331.
(31) Wang, X.; Liu, Z.; Sui, X.; Wu, Q.; Wang, J.; Xu, C. Elemene injection as adjunctive treatment to platinum-based chemotherapy in patients with stage iii/iv non-small cell lung cancer: A meta-analysis following the PRISMA guidelines. *Phytomedicine* **2019**, *59*, No. 152787.
(32) Tenchov, R.; Bird, R.; Curtze, A. E.; Zhou, Q. Lipid nanoparticles horizontal line from liposomes to mRNA vaccine delivery, a landscape of research diversity and advancement. *ACS Nano* **2021**, *15* (11), 16982−17015.
(33) Gajbhiye, K. R.; Salve, R.; Narwade, M.; Sheikh, A.; Kesharwani, P.; Gajbhiye, V. Lipid polymer hybrid nanoparticles: A custom-tailored next-generation approach for cancer therapeutics. *Mol. Cancer* **2023**, *22* (1), No. 160.
(34) Li, Y.; Wu, P.; Zhu, M.; Liang, M.; Zhang, L.; Zong, Y.; Wan, M. High-performance delivery of a CRISPR interference system via lipid-polymer hybrid nanoparticles combined with ultrasound-mediated microbubble destruction for tumor-specific gene repression. *Adv. Healthcare Mater.* **2023**, *12* (10), No. 2203082.
(35) Wang, X.; Gu, H.; Zhang, H.; Xian, J.; Li, J.; Fu, C.; Zhang, C.; Zhang, J. Oral core-shell nanoparticles embedded in hydrogel microspheres for the efficient site-specific delivery of magnolol and enhanced antiulcerative colitis therapy. *ACS Appl. Mater. Interfaces* **2021**, *13* (29), 33948−33961.
(36) Li, J.; Mooney, D. J. Designing hydrogels for controlled drug delivery. *Nat. Rev. Mater.* **2016**, *1* (12), No. 16071.
(37) Pan, J.; Liao, H.; Gong, G.; He, Y.; Wang, Q.; Qin, L.; Zhang, Y.; Ejima, H.; Tardy, B. L.; Richardson, J. J.; Shang, J.; Rojas, O. J.; Zeng, Y.; Guo, J. Supramolecular nanoarchitectonics of phenolic-based nanofiller for controlled diffusion of versatile drugs in hydrogels. *J. Controlled Release* **2023**, *360*, 433−446.
(38) Choi, S. W.; Guan, W.; Chung, K. Basic principles of hydrogel-based tissue transformation technologies and their applications. *Cell* **2021**, *184* (16), 4115−4136.
(39) Luo, Z.; Wang, Y.; Li, J.; Wang, J.; Yu, Y.; Zhao, Y. Tailoring hyaluronic acid hydrogels for biomedical applications. *Adv. Funct. Mater.* **2023**, *33* (49), No. 2306554.
(40) Tavakoli, S.; Krishnan, N.; Mokhtari, H.; Oommen, O. P.; Varghese, O. P. Fine-tuning dynamic cross-linking for enhanced 3d bioprinting of hyaluronic acid hydrogels. *Adv. Funct. Mater.* **2024**, *34* (4), No. 2307040.

https://doi.org/10.1021/jacs.4c12531
J. Am. Chem. Soc. XXXX, XXX, XXX−XXX

(41) Burdick, J. A.; Prestwich, G. D. Hyaluronic acid hydrogels for biomedical applications. *Adv. Mater.* **2011**, *23* (12), H41−H56.
(42) Zhou, D.; Li, S.; Pei, M.; Yang, H.; Gu, S.; Tao, Y.; Ye, D.; Zhou, Y.; Xu, W.; Xiao, P. Dopamine-modified hyaluronic acid hydrogel adhesives with fast-forming and high tissue adhesion. *ACS Appl. Mater. Interfaces* **2020**, *12* (16), 18225−18234.
(43) Guimarães, C. F.; Gasperini, L.; Marques, A. P.; Reis, R. L. The stiffness of living tissues and its implications for tissue engineering. *Nat. Rev. Mater.* **2020**, *5* (5), 351−370.
(44) Bruschi, M. L. *Strategies to Modify the Drug Release from Pharmaceutical.*; Elsevier: Cambridge, MA, USA, 2015.
(45) Neves, B. S.; Gonçalves, R. C.; Mano, J. F.; Oliveira, M. B. Controlling the diffusion of small molecules from matrices processed by all-aqueous methodologies: Towards the development of green pharmaceutical products. *Green Chem.* **2024**, *26* (8), 4417−4431.
(46) Na, T.-Y.; Schecterson, L.; Mendonsa, A. M.; Gumbiner, B. M. The functional activity of E-cadherin controls tumor cell metastasis at multiple steps. *Proc. Natl. Acad. Sci. U.S.A.* **2020**, *117* (11), 5931−5937.
(47) Tian, Y.; Wang, Z.; Cao, S.; Liu, D.; Zhang, Y.; Chen, C.; Jiang, Z.; Ma, J.; Wang, Y. Connective tissue inspired elastomer-based hydrogel for artificial skin via radiation-indued penetrating polymerization. *Nat. Commun.* **2024**, *15* (1), No. 636.
(48) Gao, C.; Cheng, K.; Li, Y.; Gong, R.; Zhao, X.; Nie, G.; Ren, H. Injectable immunotherapeutic hydrogel containing RNA-loaded lipid nanoparticles reshapes tumor microenvironment for pancreatic cancer therapy. *Nano Lett.* **2022**, *22* (22), 8801−8809.
(49) Mi, D.; Li, J.; Wang, R.; Li, Y.; Zou, L.; Sun, C.; Yan, S.; Yang, H.; Zhao, M.; Shi, S. Postsurgical wound management and prevention of triple-negative breast cancer recurrence with a pyroptosis-inducing, photopolymerizable hydrogel. *J. Controlled Release* **2023**, *356*, 205−218.
(50) Zhu, Y.; Jin, L.; Chen, J.; Su, M.; Sun, T.; Yang, X. Promoting the recruitment, engagement, and reinvigoration of effector T cells via an injectable hydrogel with a supramolecular binding capability for cancer immunotherapy. *Adv. Mater.* **2023**, *35* (47), No. e2309667.
(51) Mantovani, A.; Allavena, P.; Marchesi, F.; Garlanda, C. Macrophages as tools and targets in cancer therapy. *Nat. Rev. Drug Discovery* **2022**, *21* (11), 799−820.
(52) Xia, Y.; Rao, L.; Yao, H.; Wang, Z.; Ning, P.; Chen, X. Engineering macrophages for cancer immunotherapy and drug delivery. *Adv. Mater.* **2020**, *32* (40), No. 2002054.
(53) Liu, Y.; Jiang, Z. Y.; Zhou, Y. L.; Qiu, H. H.; Wang, G.; Luo, Y.; Liu, J. B.; Liu, X. W.; Bu, W. Q.; Song, J.; Cui, L.; Jia, X. B.; Feng, L. β-elemene regulates endoplasmic reticulum stress to induce the apoptosis of NSCLC cells through PERK/IRE1α/ATF6 pathway. *Biomed. Pharmacother.* **2017**, *93*, 490−497.

https://doi.org/10.1021/jacs.4c12531
J. Am. Chem. Soc. XXXX, XXX, XXX−XXX